***The following resources related to this article are available online at
www.sciencemag.org (this information is current as of February 15, 2013):***

Updated information and services, including high-resolution figures, can be found in the online version of this article at:
http://www.sciencemag.org/content/317/5836/372.full.html

Supporting Online Material can be found at:
http://www.sciencemag.org/content/suppl/2007/07/17/317.5836.372.DC1.html

A list of selected additional articles on the Science Web sites **related to this article** can be found at:
http://www.sciencemag.org/content/317/5836/372.full.html#related

This article **cites 16 articles**, 7 of which can be accessed free:
http://www.sciencemag.org/content/317/5836/372.full.html#ref-list-1

This article has been **cited by** 150 article(s) on the ISI Web of Science

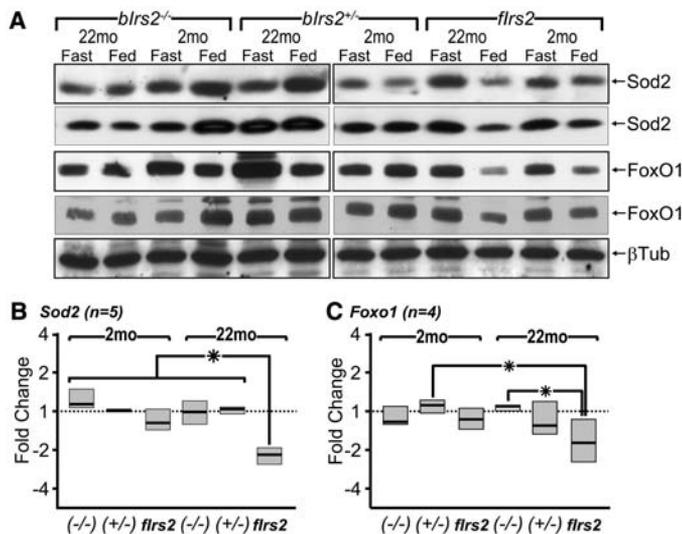This article has been **cited by** 100 articles hosted by HighWire Press; see:
http://www.sciencemag.org/content/317/5836/372.full.html#related-urls

This article appears in the following **subject collections:**
Cell Biology
http://www.sciencemag.org/cgi/collection/cell_biol

Fig. 4. Loss of brain Irs2 stabilizes Sod2 in the postprandial brain. (**A**) Hypothalamic lysates were prepared from pairs of male siblings of the indicated genotype before (Fast) or after 2-hour feeding (Fed), resolved by SDS polyacrylamide gel electrophoresis, and immunoblotted with antibodies against Sod2 or FoxO1 (two independent experiments are shown). β-tubulin (shown for one experiment) was immunoblotted for all the experiments to confirm equivalent loading. Autoradiographs were quantified, and the ratio of intensities (Fed/Fast) for (**B**) Sod2 ($n = 5$) or (**C**) FoxO1 ($n = 4$) was calculated. Boxes show the median ratio (solid horizontal line) and the lower and upper quartiles; the Kruskal-Wallis nonparametric test was used to compare the groups across all genotypes (*$P < 0.05$).

References and Notes

1. K. A. Hughes, R. M. Reynolds, *Annu. Rev. Entomol.* **50**, 421 (2005).
2. R. A. Miller, *J. Am. Geriatr. Soc.* **53**, S284 (2005).
3. C. Kenyon, *Cell* **120**, 449 (2005).
4. D. A. Sinclair, L. Guarente, *Sci. Am.* **294**, 48 (2006).
5. M. S. Bonkowski, J. S. Rocha, M. M. Masternak, K. A. Al Regaiey, A. Bartke, *Proc. Natl. Acad. Sci. U.S.A.* **103**, 7901 (2006).
6. M. F. White, *Science* **302**, 1710 (2003).
7. D. J. Clancy *et al.*, *Science* **292**, 104 (2001).
8. D. S. Hwangbo, B. Gershman, M. P. Tu, M. Palmer, M. Tatar, *Nature* **429**, 562 (2004).
9. D. J. Withers *et al.*, *Nature* **391**, 900 (1998).
10. D. J. Withers *et al.*, *Nat. Genet.* **23**, 32 (1999).
11. D. W. Hosmer Jr., S. Lemeshow, *Applied Survival Analysis* (Wiley, New York, 1999).
12. R. W. Gelling *et al.*, *Cell Metab.* **3**, 67 (2006).
13. X. Lin *et al.*, *J. Clin. Investig.* **114**, 908 (2004).
14. T. L. Parkes *et al.*, *Nat. Genet.* **19**, 171 (1998).
15. C. A. Wolkow, K. D. Kimura, M.-S. Lee, G. Ruvkum, *Science* **290**, 147 (2000).
16. D. J. Burks *et al.*, *Nature* **407**, 377 (2000).
17. A. I. Choudhury *et al.*, *J. Clin. Investig.* **115**, 940 (2005).
18. M. Schubert *et al.*, *J. Neurosci.* **23**, 7084 (2003).
19. Y. Wang *et al.*, *Physiol. Genomics* **27**, 131 (2006).
20. M. R. Rizzo *et al.*, *J. Clin. Endocrinol. Metab.* **90**, 409 (2005).
21. H. Kabil, L. Partridge, L. G. Harshman, *Biogerontology* **8**, 201 (2007).
22. R. A. Miller, J. M. Harper, A. Galecki, D. T. Burke, *Aging Cell* **1**, 22 (2002).
23. M. Barbieri *et al.*, *Exp. Gerontol.* **38**, 137 (2003).
24. We thank R. Leshan, K. Martin, C. Aubin, N. Fujii, and V. Petkovana for technical assistance and C. Lee, J. Elmquist, M. Anderson, and H. Feldman for helpful advice. This work was supported by NIH (grants DK55326 and DK38712 to M.F.W.), the Japan Society for the Promotion of Science (A.T.), and the Yamada Science Foundation (A.T.). M.F.W. is an investigator at the Howard Hughes Medical Institute.

However, our long-lived mice are slightly larger and consume about the same or slightly more food than the short-lived controls. Indeed, long-lived systemic $Irs2^{+/-}$ mice are more insulin sensitive and glucose tolerant than WT mice; however, long-lived brain-specific $bIrs2^{+/-}$ and $bIrs2^{-/-}$ mice are insulin resistant, hyperinsulinemic, and glucose intolerant. The mechanism responsible for this disparity is unknown. Regardless, our results point to the brain as the site where reduced insulin-like signaling can have a consistent effect to extend mammalian life span—as it does in *C. elegans* and *D. melanogaster* (*1, 3*).

As mammals age, compensatory hyperinsulinemia usually develops to maintain glucose homeostasis and prevent the progression toward life-threatening type 2 diabetes (*6*); however, increased circulating insulin might have negative effects on the brain that can reduce life span (*4, 21, 23*). By directly attenuating brain Irs2 signaling, an aging brain can be shielded from the negative effects of hyperinsulinemia that ordinarily develop with overweight and advancing age. Consistent with this hypothesis, moderate daily exercise, calorie restriction, and weight loss—which reduce circulating insulin—might increase life span by attenuating Irs2 signaling in the brain. Other strategies that improve peripheral insulin sensitivity, such as reduced growth hormone signaling, could have the same effect (*5*). Indeed, human centenarians display increased peripheral insulin sensitivity and reduced circulating insulin concentrations (*23*). Hence, we suggest that the Irs2 signaling cascade in the brain integrates the effects of peripheral nutrient homeostasis with life span.

Patched1 Regulates Hedgehog Signaling at the Primary Cilium

Rajat Rohatgi,[1,2]* Ljiljana Milenkovic,[1]* Matthew P. Scott[1]†

Primary cilia are essential for transduction of the Hedgehog (Hh) signal in mammals. We investigated the role of primary cilia in regulation of Patched1 (Ptc1), the receptor for Sonic Hedgehog (Shh). Ptc1 localized to cilia and inhibited Smoothened (Smo) by preventing its accumulation within cilia. When Shh bound to Ptc1, Ptc1 left the cilia, leading to accumulation of Smo and activation of signaling. Thus, primary cilia sense Shh and transduce signals that play critical roles in development, carcinogenesis, and stem cell function.

The Hedgehog (Hh) signaling pathway plays an important role both in embryonic development and in adult stem cell function (*1, 2*). Dysregulation of the pathway causes birth defects and human cancer (*2*). Despite the importance of Hh signaling in mammals, there are gaps in our understanding of early events in this pathway. In the absence of signal, the transmembrane protein Patched1 (Ptc1) keeps the pathway turned off by inhibiting the function of a second transmembrane protein, Smoothened (Smo). The secreted protein Sonic Hedgehog (Shh) binds and inactivates Ptc1, allowing activation of Smo. Smo then triggers target gene transcription through the Gli family of transcription factors. The mechanism by which Shh inhibits Ptc1 and Ptc1 inhibits Smo is not understood in mammals.

In *Drosophila*, Ptc inhibits the movement of Smo to the plasma membrane. Binding of Hh causes the internalization of Ptc from the plasma

[1]Departments of Developmental Biology, Genetics, and Bioengineering and Howard Hughes Medical Institute, Stanford University School of Medicine, Stanford, CA 94305, USA. [2]Department of Oncology, Stanford University School of Medicine, Stanford, CA 94305, USA.

*These authors contributed equally to this work.
†To whom correspondence should be addressed. E-mail: mscott@stanford.edu

membrane to vesicles, allowing Smo to translocate to the plasma membrane and activate downstream signaling (*3*, *4*). The discovery that protein components of primary cilia are required for Hh signaling suggested that subcellular localization has an important role in mammalian Hh signaling (*5*). Primary cilia are cell surface projections found on most vertebrate cells that function as sensory "antennae" for signals (*6*). Several components of the Hh pathway, including Smo and the Gli proteins, accumulate in primary cilia, and Smo is enriched in cilia upon stimulation with Shh (*7*, *8*).
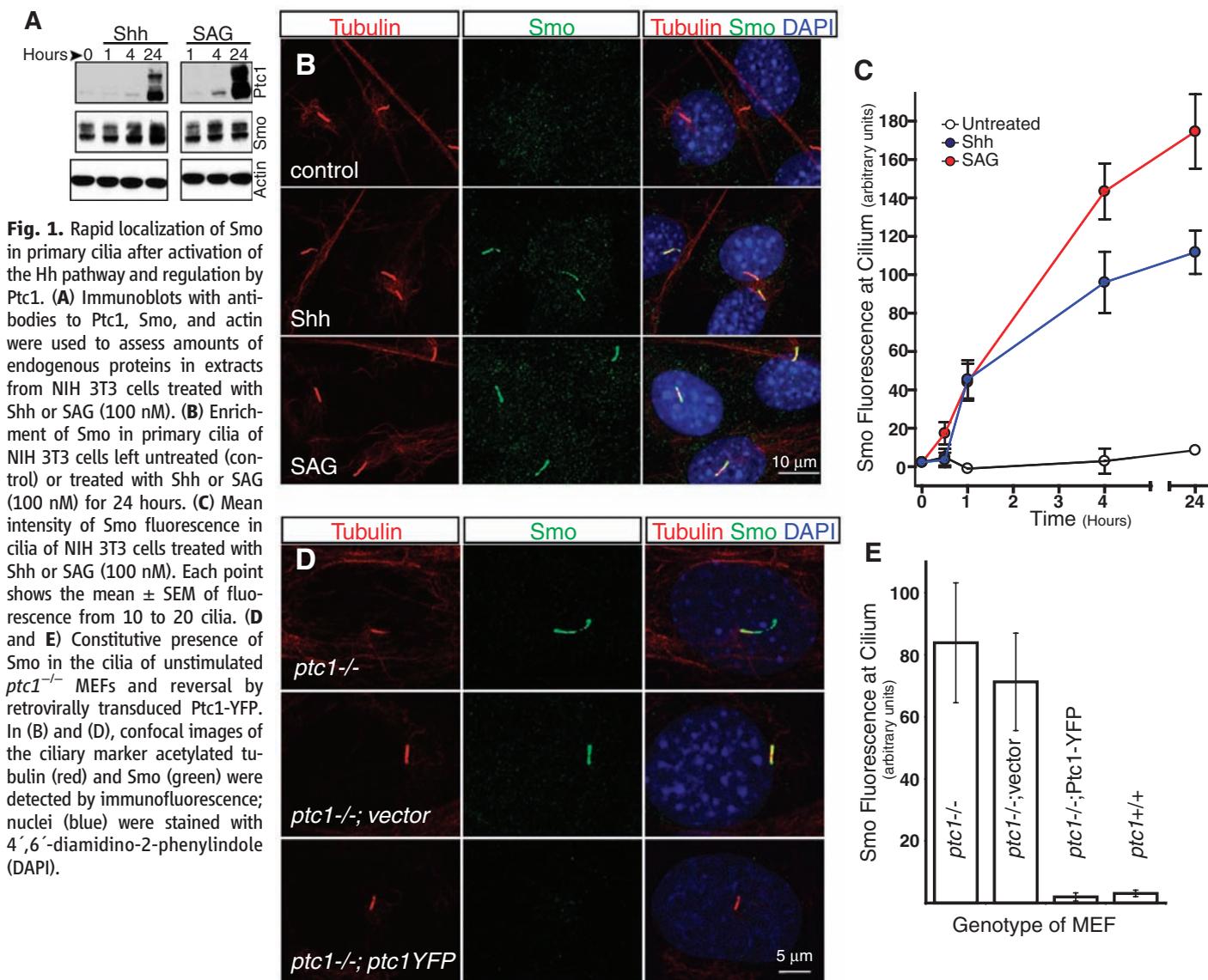
We examined the dynamic subcellular localization of Ptc1 and Smo in mammalian cells with the use of novel antibodies to the two proteins (fig. S1). These antibodies allowed detection of endogenous Ptc1 and Smo in cultured mouse fibroblasts (NIH 3T3 cells) and mouse embryonic fibroblasts (MEFs), two Hh-responsive cell types (*9*). Hh signaling was activated in NIH 3T3 cells by treatment with either Shh or SAG (Shh-agonist),

a small molecule that directly binds and activates Smo (*10*). Because *ptc1* is itself a transcriptional target of Hh signaling, increases in Ptc1 protein levels can serve as a metric for pathway activation. Ptc1 protein levels began to rise by 4 hours and continued to increase until 24 hours after addition of Shh (Fig. 1A). After stimulation of cells with Shh or SAG, endogenous Smo was enriched in primary cilia (Fig. 1B). The mean fluorescence intensity of Smo in cilia began to increase as early as 1 hour after stimulation of cells with Shh or SAG (Fig. 1C and fig. S2). This likely represented relocalization from a cytoplasmic pool, because the total amount of Smo protein did not increase at this time point (Fig. 1A).

To determine whether Ptc1 regulates the localization of Smo, we examined Smo localization in MEFs from *ptc1*−/− mice (*9*). These cells showed constitutive activation of Hh target gene transcription (fig. S3). Consistent with a role of Ptc1 in regulating Smo trafficking, Smo was constitutively localized to primary cilia in

these cells even in the absence of Shh or SAG (Fig. 1, D and E). Reintroduction of Ptc1 into these cells by means of a retrovirus suppressed Hh-pathway activity (fig. S3) and prevented Smo accumulation in primary cilia (Fig. 1, D and E). Thus, the regulation of Smo localization by Ptc1 is conserved from flies to mammals.

To understand how Ptc1 may regulate entry of Smo into the cilium, we examined the localization of Ptc1 in MEFs and mouse embryos. Endogenous Ptc1 was present in small amounts in MEFs, near the limit of detection by immunofluorescence. We therefore increased the amounts of Ptc1 protein by stimulating cells with SAG. Under these conditions, Ptc1 was highly enriched in primary cilia (Fig. 2A). The ciliary localization of Ptc1 was confirmed in three additional ways. First, Ptc1 fused to yellow fluorescent protein (Ptc1-YFP) was found around the base and in the shaft of cilia in unstimulated *ptc1*−/− cells infected with a retrovirus encoding Ptc1-YFP (Figs. 2B and fig. S12). Second, Ptc1-YFP overproduced


Fig. 1. Rapid localization of Smo in primary cilia after activation of the Hh pathway and regulation by Ptc1. (**A**) Immunoblots with antibodies to Ptc1, Smo, and actin were used to assess amounts of endogenous proteins in extracts from NIH 3T3 cells treated with Shh or SAG (100 nM). (**B**) Enrichment of Smo in primary cilia of NIH 3T3 cells left untreated (control) or treated with Shh or SAG (100 nM) for 24 hours. (**C**) Mean intensity of Smo fluorescence in cilia of NIH 3T3 cells treated with Shh or SAG (100 nM). Each point shows the mean ± SEM of fluorescence from 10 to 20 cilia. (**D** and **E**) Constitutive presence of Smo in the cilia of unstimulated *ptc1*−/− MEFs and reversal by retrovirally transduced Ptc1-YFP. In (B) and (D), confocal images of the ciliary marker acetylated tubulin (red) and Smo (green) were detected by immunofluorescence; nuclei (blue) were stained with 4′,6′-diamidino-2-phenylindole (DAPI).

in $ptc1^{-/-}$ cells by transfection showed clear ciliary localization in both live and fixed cells (Fig. 3A and figs. S10 and S14). Third and most important, endogenous Ptc1 was found in the cilia of mouse embryo mesoderm cells responsive to Shh (Fig. 2D and figs. S4 and S5) (1).

Ptc1 staining in cross sections of embryonic day 9.5 (E9.5) embryos was detected in cells of the ventral neural tube, notochord, splanchnic mesoderm, and paraxial mesoderm, precisely the regions where Hh signaling is known to be active and Shh target genes such as ptc1 are highly expressed (Fig. 2C and fig. S4B) (1). We focused on mesoderm cells because they are likely the cells that gave rise to the MEFs that we have analyzed in culture. Endogenous Ptc1 showed asymmetric localization to a domain surrounding the base of the cilium and in particles along the shaft of the cilium (Fig. 2D and figs. S4C and S5). This localization pattern around the base and in a particulate pattern along the shaft of the cilium is similar to that seen in cultured fibroblasts (compare Fig. 2D and fig. S12). In embryo cells, there was more variability in the amount of Ptc1 in the shaft of cilia, a finding likely related to differences in the amount of Shh signal received by cells in the complex milieu of embryonic tissue. The concentration of Ptc1 at the base of primary cilia suggests a mechanism for how it may inhibit Smo activation. Transport of proteins in and out of primary cilia is thought to be regulated at their base, and Ptc1 could function at this location to inhibit a protein-trafficking step critical for Smo activation (11).

Shh could inactivate Ptc1 by binding to it at the cilium and inducing its internalization, degradation, or movement to other regions of the plasma membrane. To determine whether Ptc1 at the cilium can bind to Shh, we produced a fluorescently labeled version of the N-terminal signaling fragment of Shh (ShhN-A594). Minute amounts of ShhN-A594, one-hundredth of those required to activate signaling, were added to live $ptc1^{-/-}$ cells transfected with Ptc1-YFP and a marker for cilia, inversin fused to cyan fluorescent protein (inversin-CFP) (12). Live cells were used because the interaction between Shh and Ptc1 does not survive fixation. ShhN-A594 concentrated at cilia containing Ptc1-YFP and colocalized with puncta of Ptc1-YFP (Fig. 3A and fig. S7). $Ptc1^{-/-}$ cells expressing inversin-CFP alone did not bind ShhN-A594, and an excess of unlabeled ShhN prevented binding of ShhN-A594 (fig. S7).

We next asked whether the interaction of Shh with Ptc1 influences the localization of Ptc1. Ptc1 was concentrated at cilia after treatment of cells with SAG alone but not after treatment with Shh or a combination of Shh and SAG (Fig. 3B). This suggested that Shh binding might trigger the removal of the Ptc1-Shh complex from the cilium, or that new Ptc1 produced in response to Shh was not localized in the cilium. To distinguish these possibilities, we induced the production of large amounts of Ptc1 in the cilia of NIH 3T3 cells with SAG treatment and then
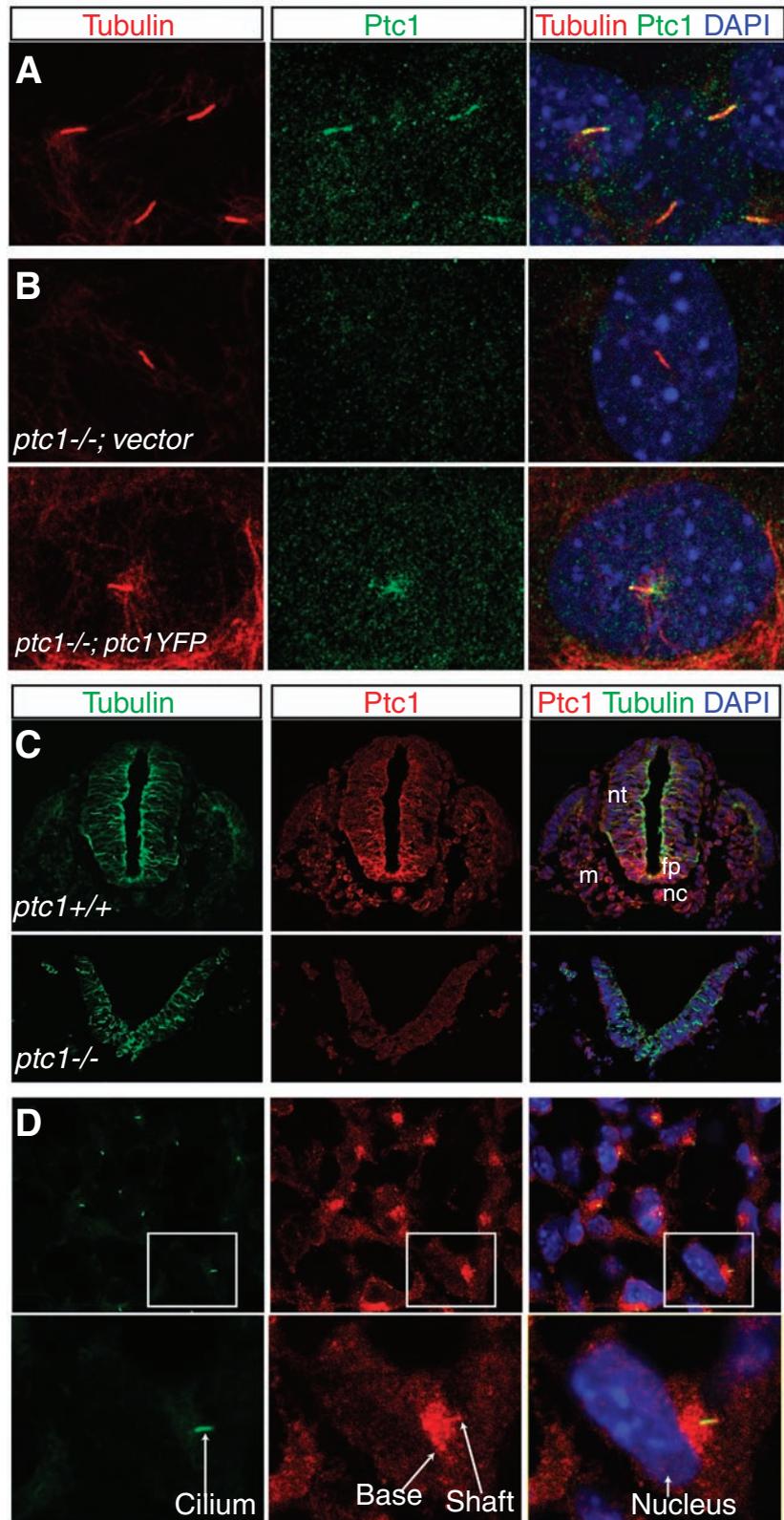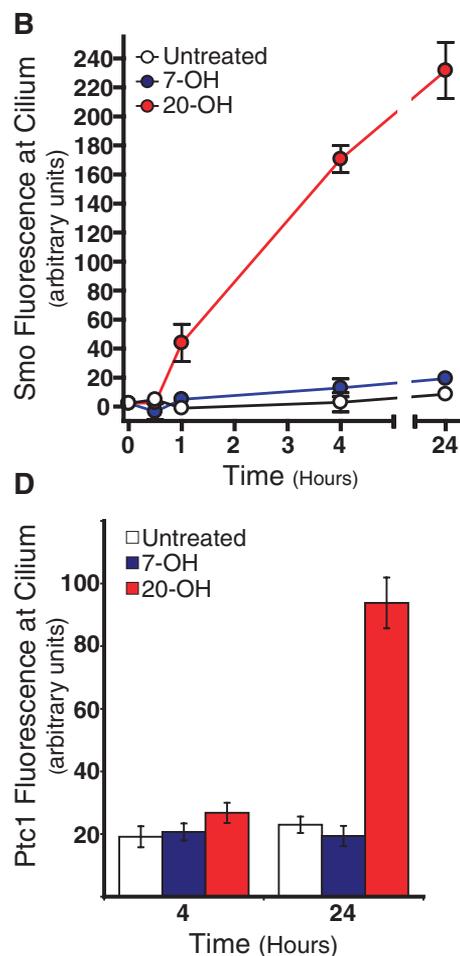

Fig. 2. Localization of Ptc1 in primary cilia. (**A**) Concentration of endogenous Ptc1 in cilia of NIH 3T3 cells stimulated with 100 nM SAG. (**B**) Localization of Ptc1-YFP in $ptc1^{-/-}$ MEFs infected with a retrovirus carrying an empty vector or the $ptc1$-YFP coding sequence. In (A) and (B), cilia (red) and Ptc1 (green) were visualized by immunofluorescence; nuclei (blue) were stained with DAPI. (**C**) Ptc1 staining in Shh-responsive cells of the neural tube (nt), notochord (nc), floor plate (fp), and paraxial mesoderm (m). Cross sections of wild-type (top row) or control $ptc1^{-/-}$ (bottom row) mouse embryos (E9.5) were imaged with a 40× objective. (**D**) Asymmetric, ciliary localization of Ptc1 in paraxial mesoderm cells. The cell boxed in white is magnified in the bottom panel; arrows indicate Ptc1 staining (red) around the base and in the shaft of cilia (green).
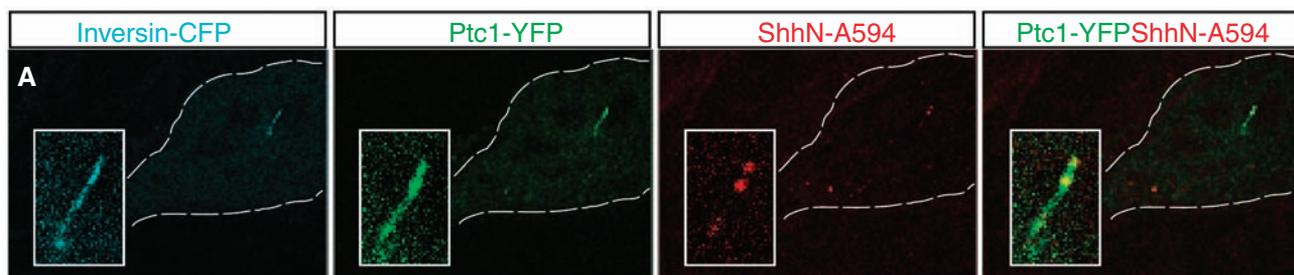
Fig. 3. Interactions between Shh and Ptc1 at primary cilia. (**A**) Colocalization of Shh and Ptc1 at the cilium shown in a confocal image of a live *ptc1⁻/⁻* cell transfected with Ptc1-YFP (green) and incubated with ShhN-A594 (red, 300 ng/ml) for 45 min. Inversin-CFP (cyan) marks the cilium, the dotted line demarcates the cell border, and insets show magnified views of the cilia. (**B**) Mean Ptc1 fluorescence in cilia of NIH 3T3 cells treated with SAG (100 nM), Shh, or both. (**C**) Disappearance of Ptc1 from primary cilia after Shh treatment. NIH 3T3 cells preincubated with SAG for 24 hours were switched to control medium (untreated) or into Shh-containing medium. The red dashed baseline shows the amount of ciliary Ptc1 in cells treated with Shh for 4 hours without a 24-hour SAG pulse.
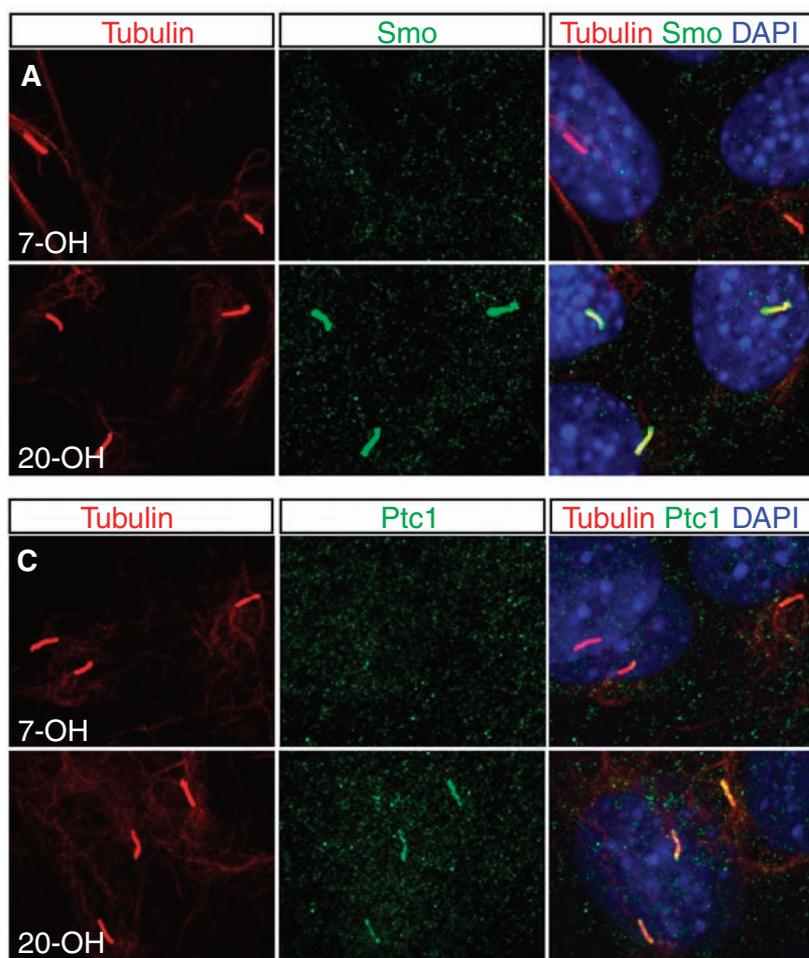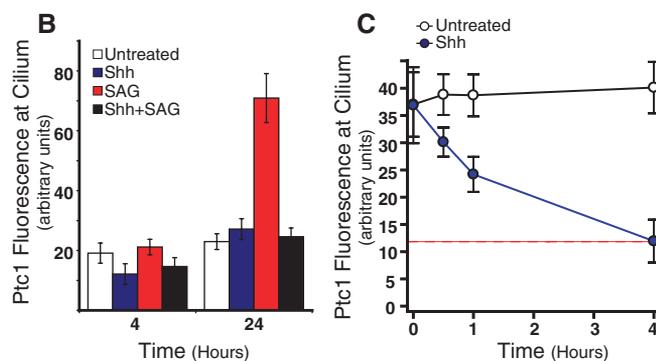
Fig. 4. Accumulation of Smo and Ptc1 at cilia of NIH 3T3 cells exposed to 20α-hydroxycholesterol. (**A** and **C**) Localization of cilia (red) and Smo or Ptc1 (green) in cells treated with 10 μM 20α-hydroxycholesterol or 7α-hydroxycholesterol for 24 hours. (**B**) Time course of Smo accumulation at the primary cilium in NIH 3T3 cells treated with 20α-hydroxycholesterol. (**D**) Increase in Ptc1 fluorescence in primary cilia after treatment with 20α-hydroxycholesterol. In (B) and (D), each point shows the mean ± SEM of fluorescence from 10 to 20 cilia.

switched the cells to control medium or medium containing Shh (Fig. 3C). Ptc1 levels in the cilium remained stable in the control, but Shh treatment caused a time-dependent disappearance of Ptc1 from the primary cilium (Fig. 3C and fig. S8). The loss of Ptc1 from cilia was not associated with a decrease in total Ptc1 protein levels (fig. S11) and thus implied movement of Ptc1 from cilia to another location in the cell. This delocalization was only evident with the endogenous protein and not upon examination of transfected Ptc1-YFP, a far more abundant protein (fig. S7B).

We measured Ptc1 and Smo localization (Figs. 1 and 3) in the same experiment. Because the localization changes for Ptc1 and Smo described above were each seen in >80% of the cilia visualized, the levels of Ptc1 and Smo in cilia were inversely correlated. The reciprocal time courses of Ptc1 disappearance and Smo appearance at cilia after Shh addition (Figs. 1C and 3C) support a model in which Shh triggers the removal of Ptc1 from the cilium, allowing Smo to enter and activate signaling. Consistent with this idea, cells of the ventral neural tube and floor plate, which receive large amounts of Shh, showed high levels of Smo and low levels of Ptc1 in cilia (fig. S13). The movement of Ptc1 and Smo at the cilium is analogous to the situation in *Drosophila*, where pathway activation is associated with Smo movement to the plasma membrane and movement of Ptc away (*3*).

Ptc1 may regulate Smo localization through a small molecule (*13*). Because Smo translocation to the primary cilium appears to be a critical step in its activation, a regulatory small molecule would be predicted to control this step. Naturally occurring oxysterols are good candidates for

endogenous small molecules that regulate Smo function. Cellular sterol concentrations are important determinants of a cell's responsiveness to Shh, and oxysterols can activate Hh signaling (*14–16*). When we treated NIH 3T3 cells with activating concentrations of the oxysterol 20α-hydroxycholesterol, Smo rapidly translocated to the primary cilium with kinetics that were identical to those seen in cells treated with SAG or Shh (Fig. 4, A and B, and fig. S9). Treatment with 7β-hydroxycholesterol, an oxysterol that does not activate the Hh pathway, did not induce translocation of Smo. This result provides a specific molecular mechanism—Smo translocation to cilia—to explain how oxysterols regulate Hh signaling.

Cells treated with 20α-hydroxycholesterol also retained Ptc1 in cilia in a pattern similar to that seen in cells treated with SAG (Fig. 4, C and D). Thus, oxysterols appear to function not like Shh, by causing the removal of Ptc1 from cilia, but at a more downstream step to make Smo insensitive to the inhibitory effects of Ptc1. However, oxysterols function differently from SAG because they likely do not directly bind to Smo (*16*).

Our results suggest that Ptc1 localization to primary cilia inhibits the Hh pathway by excluding Smo and also allows cilia to function as chemosensors for the detection of extracellular Shh. Binding of Shh to Ptc1 at primary cilia is coupled to pathway activation by the reciprocal movement of Ptc1 out of the cilia and Smo into the cilia, a process that may be mediated by oxysterols. Elucidating the molecular machinery that controls Ptc1 and Smo trafficking at primary cilia will likely provide new targets for modulation of this important pathway.

References and Notes

1. P. W. Ingham, A. P. McMahon, *Genes Dev.* **15**, 3059 (2001).
2. P. A. Beachy, S. S. Karhadkar, D. M. Berman, *Nature* **432**, 324 (2004).
3. A. J. Zhu, L. Zheng, K. Suyama, M. P. Scott, *Genes Dev.* **17**, 1240 (2003).
4. N. Denef, D. Neubuser, L. Perez, S. M. Cohen, *Cell* **102**, 521 (2000).
5. D. Huangfu *et al.*, *Nature* **426**, 83 (2003).
6. V. Singla, J. F. Reiter, *Science* **313**, 629 (2006).
7. K. C. Corbit *et al.*, *Nature* **437**, 1018 (2005).
8. C. J. Haycraft *et al.*, *PLoS Genet.* **1**, e53 (2005).
9. J. Taipale *et al.*, *Nature* **406**, 1005 (2000).
10. J. K. Chen, J. Taipale, K. E. Young, T. Maiti, P. A. Beachy, *Proc. Natl. Acad. Sci. U.S.A.* **99**, 14071 (2002).
11. J. L. Rosenbaum, G. B. Witman, *Nat. Rev. Mol. Cell Biol.* **3**, 813 (2002).
12. D. Watanabe *et al.*, *Development* **130**, 1725 (2003).
13. J. Taipale, M. K. Cooper, T. Maiti, P. A. Beachy, *Nature* **418**, 892 (2002).
14. M. K. Cooper *et al.*, *Nat. Genet.* **33**, 508 (2003).
15. R. B. Corcoran, M. P. Scott, *Proc. Natl. Acad. Sci. U.S.A.* **103**, 8408 (2006).
16. J. R. Dwyer *et al.*, *J. Biol. Chem.* **282**, 8959 (2007).
17. M.P.S. is an investigator of the Howard Hughes Medical Institute and is supported by National Cancer Institute grant R01 CA088060. R.R. is a Robert Black Fellow of the Damon Runyon Cancer Research Fund (DRG 103-06). We thank R. Corcoran for discussions of oxysterol effects, P. Beachy for smo⁻/⁻ cells and for sharing results before publication, J. Chen for SAG, O. Brandman for image analysis advice, J. Hyman for microscopy advice, R. Johnson and K. Suyama for Ptc1 antiserum, H. Hamada for inversin constructs, D. Ko for the Ptc1-YFP construct, A. Salic for the Shh labeling strategy, and T. Hillman, C. Ho, A. Kumar, and A. Balmain for comments.

Host Immune System Gene Targeting by a Viral miRNA

Noam Stern-Ginossar,[1]* Naama Elefant,[2]* Albert Zimmermann,[3] Dana G. Wolf,[4] Nivin Saleh,[4] Moshe Biton,[1] Elad Horwitz,[1] Zafnat Prokocimer,[1] Mark Prichard,[5] Gabriele Hahn,[6]† Debra Goldman-Wohl,[7] Caryn Greenfield,[7] Simcha Yagel,[7] Hartmut Hengel,[3] Yael Altuvia,[2]‡ Hanah Margalit,[2]*‡ Ofer Mandelboim[1]*‡

Virally encoded microRNAs (miRNAs) have recently been discovered in herpesviruses. However, their biological roles are mostly unknown. We developed an algorithm for the prediction of miRNA targets and applied it to human cytomegalovirus miRNAs, resulting in the identification of the major histocompatibility complex class I–related chain B (MICB) gene as a top candidate target of hcmv-miR-UL112. MICB is a stress-induced ligand of the natural killer (NK) cell activating receptor NKG2D and is critical for the NK cell killing of virus-infected cells and tumor cells. We show that hcmv-miR-UL112 specifically down-regulates MICB expression during viral infection, leading to decreased binding of NKG2D and reduced killing by NK cells. Our results reveal a miRNA-based immunoevasion mechanism that appears to be exploited by human cytomegalovirus.

MiRNAs constitute a large family of small noncoding RNAs that regulate gene expression posttranscriptionally, affecting mRNA degradation and translation by base-pairing with the 3′ untranslated regions (3′UTRs) (*1*). The recent discovery of virally encoded miRNAs, mostly in herpesviruses, intriguingly suggests that miRNAs may function in interspecies regulation involving viral miRNAs and host genes (*2–4*). Human cytomegalovirus

(HCMV) is known to have evolved effective immune evasion strategies, encoding many immunomodulatory proteins that manipulate the immune response (*5*, *6*). It is thus conceivable that miRNAs encoded by HCMV (*2*) might be exploited during immune evasion. To test this hypothesis, we sought to identify potential human target genes of the HCMV miRNAs by using our newly developed target prediction algorithm,

[1]Lautenberg Center for General and Tumor Immunology, Hebrew University Hadassah Medical School, Jerusalem, Israel. [2]Department of Molecular Genetics and Biotechnology, Hebrew University Hadassah Medical School, Jerusalem, Israel. [3]Institute for Virology, Heinrich Heine University, D40225 Düsseldorf, Germany. [4]Department of Clinical Microbiology and Infectious Diseases, Hadassah University Hospital, Jerusalem, Israel. [5]Department of Pediatrics, University of Alabama, Birmingham, AL 35233, USA [6]Max von Pettenkofer Institut, Department of Virology, D80336 Munich, Germany. [7]Department of Obstetrics and Gynecology, Hadassah Hebrew University Hospital Mount Scopus, Jerusalem, Israel.

*These authors contributed equally to this work.
†Present address: Klinikum Ingolstadt, Institut für Laboratoriumsmedizin, D84049 Ingolstadt, Germany.
‡To whom correspondence should be addressed. E-mail: yaelal@md.huji.ac.il (Y.A.); hanahm@ekmd.huji.ac.il (H.M.); oferm@ekmd.huji.ac.il (O.M.)